Research Square

Preprints are preliminary reports that have not undergone peer review.
They should not be considered conclusive, used to inform clinical practice,
or referenced by the media as validated information.

Simultaneous profiling of full-length RNA transcripts and chromatin accessibility within single cells of human retinal organoids

Youjin Hu

huyoujin@gzzoc.com

Sun Yat-sen University https://orcid.org/0000-0002-7758-8733

Shuyao Zhang

Zhongshan Ophthalmic Center, Sun Yat-Sen University

Xinzhi Mo

Zhongshan Ophthalmic Center, Sun Yat-Sen University

Yuhua Xiao

Zhongshan Ophthalmic Center, Sun Yat-Sen University

Yuanhui Qiu

State Key Laboratory of Ophthalmology, Zhongshan Ophthalmic Center, Sun Yat-Sen University

Jiawei Zhong

State Key Laboratory of Ophthalmology, Zhongshan Ophthalmic Center, Sun Yat-Sen University
https://orcid.org/0000-0002-2802-0770

Zheyao Chen

Zhongshan Ophthalmic Center, Sun Yat-Sen University

Xu Liu

Zhongshan Ophthalmic Center, Sun Yat-Sen University https://orcid.org/0009-0008-4142-6864

Xu Chen

Zhongshan Ophthalmic Center, Sun Yat-Sen University

Wangxuan Dai

Zhongshan Ophthalmic Center, Sun Yat-Sen University

Jia Chen

Zhongshan Ophthalmic Center, Sun Yat-Sen University

Xishan Jin

Zhongshan Ophthalmic Center, Sun Yat-Sen University

Guoping Fan

David Geffen School of Medicine, UCLA, Los Angeles, CA

Article

Keywords: single-cell multi-omics sequencing, full-length RNA isoforms, human retinal organoids, neural cell development and regeneration

Posted Date: December 20th, 2023

DOI: https://doi.org/10.21203/rs.3.rs-3640234/v1

License: This work is licensed under a Creative Commons Attribution 4.0 International License. Read Full License

Additional Declarations: There is **NO** Competing Interest.

Version of Record: A version of this preprint was published at Nature Communications on September 13th, 2024. See the published version at https://doi.org/10.1038/s41467-024-52335-0.

Abstract

Single-cell multi-omics sequencing can integrate transcriptome and epigenome to analyze the complex mechanisms underlying neuron development and regeneration, but most current methods are based on second-generation short-read sequencing, which has low efficiency in detecting RNA structural heterogeneity. Long-length sequencing can analyze RNA structures, but the throughput and the number of transcripts detected at the single-cell level are very low, and single-cell level epigenome profiling has not been accomplished either. Therefore, there is currently a lack of an effective method that can integrate RNA splicing and epigenetic modification to analyze the molecular mechanism of neural development. This study developed a single-cell multi-omics assay based on short-read sequencing for the simultaneous detection of single-cell full-length RNA isoforms and DNA accessibility. The accuracy of its resolution in RNA transcript structure can reach 94.5%, and the sensitivity of detecting single-cell gene expression is twice that of third-generation sequencing. And it can detect over 10,000 single nuclei at one run, enabling the effective integrated analysis of single-cell RNA isoforms and DNA accessibility at high throughput. We used this method to construct a multidimensional cell atlas of human retinal organoids, and found that gene expression and differential choices of isoforms of multiple fate-determining factors were significantly associated with chromatin accessibility. This method provides a new technical method for dissecting the multidimensional molecular mechanism of fate determination in neural cell development and regeneration.

Introduction

RNA isoform diversity mediates the variable functions of individual genes, accounting for the heterogenous phenotypes among single cells. Epigenetic modifications on the genome with identical genetic information also significantly accounts for the heterogeneity among single cells within the tissues. Recently, epigenetic variation was found to mediate the differential RNA structures among single cells. However, efficient methods to profile RNA isoform and epigenetic status of individual single cells at genome wide is still lacking. Although a lot of single cell sequencing methods to profile transcriptome and epigenome have been developed[1–3], the method to simultaneously detect the RNA isoform and epigenome has not been developed.

Majority of the current single cell RNA sequencing methods were based on short-read based with a read length below 150 base pairs, which is not suitable to characterize the structures of full-length RNA. Third generation based single cell RNA sequencing methods can reveal the full-length RNA isoforms, but the high cost and low sensitivity make it less applicable to integrate into the single cell multi-omics analysis.

Previously, we developed a short-read based method scRCAT-seq to profile the diversities in TSS and TES of RNA isoforms, which requires only nanograms of cDNA as input[4]. Here, we optimized the protocol of scRCAT-seq to profile the full-length of single molecules of RNA at genome wide (scRCAT-seq2), and further integrated with single cell ATAC to simultaneous profiling chromatin accessibility and full-length RNA isoforms within the same single cells (scRICA-seq, single cell RNA isoform and chromatin

accessibility sequencing). By applying scRICA-seq to profile the multi-omic landscape of human retinal organoids, we revealed concordant regulation of chromatin accessibility and RNA spicing on key fate determinators mediating neuron development and regeneration within the human retinal organoids.

Results

The design of scRICA-seq.

To simultaneously profile chromatin accessibility, RNA expression, and transcript structure in the same cell, we employ two strategies that enable parallel capture and sequencing of DNA and RNA. Firstly, for low-throughput single-cell samples, we utilize a nuclear-cytoplasmic separation method that has been previously established by our team[5]. This method allows us to isolate cell nuclei for chromatin accessibility sequencing analysis, while the cytoplasmic RNA from the same cell is utilized for full-length transcriptome analysis. For high-throughput single-cell populations, we employ the 10x genomics microfluidic system, which enables parallel analysis of chromatin accessibility and full-length transcriptome analysis within individual cell nuclei (Fig. 1a).

To facilitate single-cell full-length transcriptome analysis, we have developed a novel method called scRCAT-seq2, which builds upon our previous work on scRCAT-seq[4]. The scRCAT-seq2 method encompasses the following steps: (1) Labeling the ends of individual RNA/cDNA molecules with a tag (barcode); (2) Creating a circular cDNA through end-to-end ligation; (3) Performing circular amplification to generate multiple copies of full-length cDNA, each with an identical tag; (4) Fragmenting the full-length cDNA by randomly inserting Tn5 transposes around the ligated ends; (5) Constructing libraries and conducting paired-end sequencing on the resulting fragments; (6) Integrating short reads with the same molecule tag to identify key features of full-length transcripts, such as transcription start sites (TSS), transcription end sites (TES), and specific exons (Fig. 1b, **Extended Data** Fig. 1).

Accuracy and sensitivity of scRCAT-seq2.

In order to assess the sensitivity and accuracy of scRCAT-seq2 in analyzing single-cell full-length transcriptomes, we introduced the RNA standard set (SIRV-set 3), consisting of multiple isoforms, into a single ES cell sample. The results showed that scRCAT-seq2 can effectively captured the transcript 5' and 3' ends as well as exons of the transcripts (Fig. 2a). SIRV-set 3 comprises 7 genes and 69 isoforms, and scRCAT-seq2 successfully detected 88% of the transcripts (61 isoforms). Moreover, when compared to the actual labels of SIRV-set 3 transcripts, scRCAT-seq2 achieved an accuracy rate of 94.45% in identifying complete transcripts, with 30.78% being identified without any reference and 46.63% being identified based on the attributes of alternate isoforms documented in the reference (Fig. 2b-c, **Extended Data** Fig. 3).

When compared to scRCAT-seq2 with ScISOr-seq, a third-generation sequencing platform based on Pacbio, scRCAT-seq2 was demonstrated to detect a higher number of genes and isoforms. Specifically, scRCAT-seq2 identified 12,309 genes, while ScISOr-seq only detected 5,378 genes. Additionally, scRCAT-

seq2 revealed an average of 2,772 full-length isoforms per cell, compared to only 1,313 isoforms detected by ScISOr-seq. The number of genes and isoforms detected by scRCAT-seq2 was 2.29-fold higher (12,309 ± 719 versus 5,378 ± 1189) and 2.11-fold higher (2,772 ± 156 versus 1,313 ± 386) compared to ScISOr-seq, respectively (Fig. 2d-e). And the majority of genes and transcripts detected by ScISOr-seq were also detected by scRCAT-seq2 (Fig. 2f-g).

Furthermore, by analyzing the intersection of genes detected at different omics levels, we found that scRCAT-seq2 detected 85.9% of the genes detected by the 10x genomics scRNA-seq platform (22,937 out of 26,691), and the majority of gene and transcript promoter regions were covered by scATAC-seq (Fig. 2h). In summary, these results demonstrated the enhanced sensitivity of scRCAT-seq2 compared to third-generation sequencing methods. It provides an effective approach for integrating and analyzing the heterogeneity and correlation among RNA expression, structural differences, and chromatin accessibility in cells.

ScRICA-seq revealed the multi-dimensional landscape of the single-cell atlas of human retinal organoids.

In order to unravel the intricate molecular mechanisms underlying cell development and diseases within the central nervous system, it is vital to investigate the comprehensive regulation of chromatin accessibility, RNA transcription, and splicing across different cell types. To accomplish this, we utilized human retinal organoids as a case study and employed scRICA-seq to build a single-cell multi-dimensional atlas and data analysis workflow.

Single-cell dissociation was performed on the 45-day cultured human retinal organoids, and the isolated cell nuclei were subjected to scRICA-seq (Fig. 1b, 3a). We performed cell clustering on the single-cell multi-omics data and identified 6 clusters, and successfully detected various cell types with typical cell markers, including RPCs, RGCs, AC/HCs, PR precursors, neurogenic RPCs, and cones (Fig. 3b). Notably, the clustering results based on single-cell transcript isoform groupings showed a high degree of consistency with those obtained from scATAC-seq and scRNA-seq (Fig. 3b-d, **Extended Data** Fig. 5). In addition, we demonstrated that the differential expression of marker genes, both at the RNA and isoform levels, in different cell types was consistent with the corresponding chromatin accessibility levels. For example, the expression of THRB[6–8] in rod cells, CRX[9,10], PDE6H[11,12], and ARR3[13,14] in cones, PAX6[15,16] in AC/HCs, and GAP43[17,18], ISL1[19] in RGCs, exhibited consistency between their RNA expression patterns and chromatin accessibility levels (Fig. 3e). Furthermore, this consistency was also observed for fate-determining factors of retinal neurons, such as HES1 in neurogenic RPCs [20], SOX2[21,22] in RPCs, ATOH7[23–25] in retinal ganglion cells (RGCs), OTX2[26–28] in the PR precursor. Importantly, the RNA expression and chromatin accessibility patterns of these genes were aligned with their activity in different cell types. This suggests that chromatin accessibility plays a role in mediating the expression of marker genes and fate-determining factors.

scRICA-seq unveiled coordinated dynamics of chromatin accessibility and RNA expression during RPC differentiation.

By constructing pseudotime differentiation trajectories for RPCs, neurogenic RPCs, PR precursors, and cones (Fig. 4a), we identified notable alterations in multiple fate-determining factors at both the transcriptional and chromatin accessibility levels during the differentiation of RPCs into cones. These changes encompassed key genes such as ARR3, CRX, THRB, HES1, ASCL-1, ATOH7, and NRL (Fig. 4b-d). Although the function of many of these transcription factors as fate-determining factor promoting RPC differentiation has been widely recognized, the epigenetic regulation of these factors remains largely unknown previously. Through direct comparisons of chromatin accessibility and gene expression between RPCs and cones, we observed a simultaneous increase in both the expression levels and chromatin accessibility of fate-determining factors in cones and retinal ganglion cells (RGCs) when compared to RPCs (Fig. 4e**- j, Extended Data Fig. 6a-d**). To identify transcription factors that are specific to different stages of differentiation, we conducted motif enrichment analysis and discovered significant enrichment of motifs associated with GSC, GSC2, PITX3, OTX2, ATOH7, ISL1, and GAP43 and others (Fig. 4k-l). Alongside the previously mentioned fate-determining factors, we also identified several novel factors, including GSC and GSC2, which are known for their vital roles in embryonic development[29–31]. Additionally, PITX3, which is essential for neuronal and lens development, was identified as well. Its deficiency has been proved to lead to retinal developmental abnormalities and visual impairments[32,33].

In summary, by using scRICA-seq, we have discovered epigenetic regulation of cell fate determinants and other novel transcription factors involved in the differentiation of RPCs into different retinal neurons, such as cones and RGCs.

The chromatin accessibility correlates with the alternative usage of RNA isoforms across different cell types during RPC differentiation.

Additionally, we examined the patterns of RNA isoform use during the differentiation of retinal progenitor cells (RPCs) into various neuronal cell types. This analysis encompassed variations in alternative promoters, alternative polyadenylation, exon skipping (SE), intron retention (RI), mutually exclusive exons (MXE), and alternative 3’ / 5’ splice site events (A3SS/A5SS) [34,35]. Initially, we performed an analysis focusing on the variation in transcription start sites (TSS) and transcription end sites (TES) and identified 96 genes that exhibited significant variations in TSS, along with 66 genes showing variations in TES when comparing retinal progenitor cells (RPCs) and cones (Fig. 5a-b). Interestingly, the genes that displayed significant variations in TSS, such as THRB, BTBD8, VMP1, and SLF1, demonstrated concurrent changes in their chromatin accessibility profiles (Fig. 5c-d, **Extended Data Fig. 6c-d**). For instance, THRB exhibited a preference for longer isoforms in RPCs, while shorter isoforms were more prevalent in cones. Moreover, the ATAC signals in the vicinity of the promoters for these shorter isoforms were significantly increased in cones compared to RPCs (Fig. 5c), pointing towards a correlation between isoform selection and chromatin accessibility.

Moreover, we conducted a comparison of variable splicing patterns between retinal progenitor cells (RPCs) and cones, which uncovered exon skipping events in 463 gene loci. Specifically, 274 loci exhibited exon skipping in RPCs, while 189 loci exhibited exon skipping in cones (Fig. 5e). In the

differentiation process from RPCs to cones, we identified 93 gene loci with mutually exclusive exons and 212 loci with intron retention (Fig. 5f-g). Furthermore, our investigation unveiled 129 gene loci with alternative 3’ splice site (A3SS) events and 83 gene loci with alternative 5’ splice site (A5SS) events (Fig. 5h-i). In addition, when comparing the variation in splicing sites with the corresponding chromatin accessibility sites, we found that the majority of splicing changes were independent of chromatin accessibility. This observation was particularly evident in genes that encoded RPC-specific isoforms (e.g., GOPC, DCTN2, PTCD3) and cone-specific isoforms (e.g., RABEPK, BUD31, GUF1) (**Extended Data Fig. 6e-j**). Interestingly, we also discovered that a small proportion (0.92%) of isoforms exhibited splicing changes that corresponded to changes in chromatin accessibility at the variable splicing sites (Fig. 5j). Examples of such genes include PPP4R3A and ERI3 (Fig. 5k-l). This finding suggests a potential relationship between chromatin accessibility and RNA splicing.

Discussion

This study introduces a method that combines chromatin accessibility, RNA expression, and differential isoform choices to conduct a comprehensive analysis of the intricate mechanisms behind the diverse functions of the genome within cells. Through the example of retinal organoid development, we have presented a novel tool and framework for investigating the mechanisms involved in neuron development and regeneration. This approach offers valuable insights into these processes.

In contrast to conventional scRNA-seq methods that typically capture fragments from either the 5’ end or 3’ end of transcripts, this method offers an unprecedented opportunity to analyze differential isoform usage at the single-cell level. While a few methods, such as smart-seq[39], smart-seq2[40], and smart-seq3[41], can capture the full-length transcripts, these methods are limited in their ability to profile a large number of single cells (thousands of single nuclei) simultaneously, thereby limiting their efficiency and throughput for analysis.

Compared with the emerging method based on third-generation sequencing technology, our method has higher throughput and high sensitivity ScISOr-seq and other technologies can realize the analysis of full-length transcripts in single cells such as a large number of cells, but the average number of transcripts per single cell is only a few hundred[42–44], which is far below the level of 12,000 transcripts that can be detected by this method. Recently, SCAN-seq[45] and SCAN-seq2[46] can increase the number of transcripts detected in a single cell, but they require library construction in a single cell unit, which is labor-intensive and difficult to increase the throughput (**Supplementary Table 2**). Based on the innovation of library construction, our method takes full advantage of the mature and relatively low-cost advantages of next-generation sequencing technology to achieve high-throughput analysis of single-cell full-length RNA. More importantly, based entirely on next-generation sequencing, we have achieved the parallel analysis of chromatin accessibility and full-length RNA structure for the first time in the field.

Our method extends the analysis of RNA expression and differential isoform selection beyond genetic mutations to epigenetic changes, greatly expanding the mechanism analysis of neural development and

disease. Previously, researchers primarily examined how genetic mutations in RNA splicing factors and splicing sites contribute to transcript differences. By profiling the RNA isoforms and chromatin accessibility with the same single cells, this novel method enabled the precise linkage of the epigenetic status of key regulatory elements with expression of individual isoforms of certain genes, facilitating a more precise investigation into the epigenetic regulation of differential usages of RNA isoforms between single cells. For examples, we showed that dynamic expression of two major isoforms of THRB, which is a fate-determining factor mediating the differentiation of human retinal progenitors to retinal ganglion cells and photoreceptors, was correlated with the differential chromatin accessibility of regulatory elements.

In addition, this study offers a novel approach to understanding the functions of differential epigenetic status among single cells. Previous research could only investigate the impact of epigenetic regulation on gene expression, as it was challenging to discern how epigenetic mechanisms specifically influence the distinct expression patterns of different transcripts from the same gene across cells. This study introduces a method that correlates DNA's epigenetic modification state with expression of RNA with variable structures, differing in choices of transcription start sites (TSS), transcription end sites (TES), and splicing of exons. By doing so, this study allows us to investigate the impact of DNA epigenetic status on transcript structure and quantitative expression, enhancing our knowledge of the molecular mechanisms underlying variations in transcript structure and function across different tissue cells.

Our study also has several limitations. (1) Despite the unprecedent sensitivity to profile the full-length transcripts, scRCAT-seq2 is dependent on the genome reference to determine the differential structures among transcripts. (2) Discrimination of differential isoform usage determined by this method is dependent on the RNA references due to its limited accuracy to assemble transcripts de novo. Integration of long-read sequencing or sanger sequencing with this method would be help to construct full-length de novo transcripts. (3) The sample size is limited to reveal the functions of transcripts identified. And the functions of the novel transcripts of fate determining factors need to be validated by future studies.

Methods

Constructing the scRCAT-seq2 library and sequencing

The scRCAT-seq2 library construction involves several steps, including mRNA capture, cDNA synthesis, single-molecule self-circle formation, rolling-circle amplification, cDNA fragmentation, TSS and TES library construction, Illumina platform sequencing, and data analysis.

Firstly, the mRNA capture and cDNA synthesis steps are performed. After obtaining the single-cell suspension, the Lysis Buffer (0.4 μL 50% Poly-ethylene Glycol 8000, 0.3 μL 2% Triton-X100, 0.04 μL RNase inhibitor (40 U/μL), 0.2 μL dNTPs (10 mM), 0.02 μL Oligo(dT) primer (100 μM), 0.5 μL SIRV-Set3 (1:10000), 1.54 μL Nuclease Free Water), RT Mix (0.1 μL Tris-HCl pH8.3 (1 M), 0.12 μL NaCl (1 M), 0.1 μL

$MgCl_2$ (100 mM), 0.04 μL GTP (100 mM), 0.32 μL DTT (100 mM), 0.05 μL RNase inhibitor (40 U/μL), 0.08 μL TSO primer (100 μM), 0.04 μL Maxima H-minus RT, 0.15 μL Nuclease Free Water), and PCR Mix (5 μL KAPA HiFi HotStart ReadyMix (2x), 0.25 μL oligo primer (10 μM), 0.25 μL linker primer (10 μM), 0.5 μL Nuclease Free Water) are prepared. Then, pick up single cells through an oral pipette into PCR tubes containing 3 μL Lysis Buffer. After shaking and brief centrifugation, the tubes are incubated in a PCR machine: 72 ℃ for 10 min. The tubes are quickly placed on ice, and then 1 μL RT Mix is added. The reaction proceeds as follows: 42 ℃ for 90 min, 10 cycles of 50 ℃ for 2 min and 42 ℃ for 2 min, and 70 ℃ for 15 min. The resulting mixture is purified using 1x AMPure XP beads and eluted with 8.5 μL Nuclease Free Water. Next, 1 μL 10x ExoI Buffer and 0.5 μL ExoI (20 U/μL) are mixed with the purified mixture. The reaction proceeds as follows: 37 ℃ for 30 min, 80 ℃ for 10 min. After the reaction, the product is purified using 1x AMPure XP beads and eluted with 4 μL Nuclease Free Water. Then, 6 μL PCR Mix is added, and the reaction proceeds as follows: 98 ℃ for 3 min, 18–25 cycles of 98 ℃ for 20 s, 65 ℃ for 30 s, and 72 ℃ for 4 min, followed by 72 ℃ for 5 min.

Next, cDNA single-molecule self-circle formation is performed. 200 ng of cDNA is mixed with 6 μL 2x NEBuilder HiFi DNA Assembly Master Mix to achieve a final volume of 12 μL. The reaction is incubated at 55 ℃ for 60 min. Then, 1 μL Exonuclease I, 1 μL Exonuclease III: Lambda Exonuclease (1:10), and 2 μL 10x NEB Buffer 1 are added to the reaction, resulting in a final volume of 20 μL. The reaction is digested at 37 ℃ for 30 min and then heated at 80 ℃ for 10 min. The product is purified using 1.8x AMPure XP beads and eluted with 10 μL Nuclease Free Water.

Rolling circle amplification is then performed. The circularized cDNA is mixed with 5 μL phi29 DNA Polymerase Reaction Buffer, 2 μL dNTP (2 mM), 1 μL Recombinant Albumin (2 mg/mL), and 1 μL Phi29 primer (10 μM), and the volume is supplemented with Nuclease Free Water to reach 19 μL. The reaction proceeds as follows: 95 ℃ for 5 min, immediately followed by incubation on ice for 2 min. Then, 1 μL phi29 DNA Polymerase is added, and the mixture is incubated at 37 ℃ for 16 hours, followed by 65 ℃ for 10 min. Finally, the product is purified using 0.6x AMPure XP beads and eluted with 10 μL Nuclease Free Water to obtain linear, multi-copy cDNA.

cDNA fragmentation is performed using 50 ng of linear, multi-copy cDNA. The cDNA is mixed with 2 μL 5x Tagment Buffer L, 0.4 μL TTE Mix (4 pmol/μL), and Nuclease Free Water to achieve a final volume of 10 μL. The reaction is incubated at 55 ℃ for 10 min. The product is purified using 1x AMPure XP beads and eluted with 20 μL Nuclease Free Water to obtain fragmented cDNA.

TSS and TES library construction are performed separately using 20 μL of fragmented cDNA. For TSS library construction: 10 μL of fragmented cDNA is mixed with 1 μL Tn5-i5 primer (10 μM), 1 μL anti-tag1 primer (10 μM), 15 μL KAPA HiFi HotStart ReadyMix (2x), and Nuclease Free Water to reach a final volume of 30 μL. The reaction proceeds as follows: 98 ℃ for 3 min, 6 cycles of 98 ℃ for 20 s, 60 ℃ for 20 s, and 72 ℃ for 90 s, followed by 72 ℃ for 5 min. After purification using 1x AMPure XP beads, the resulting product is eluted with 10 μL Nuclease Free Water, yielding TSS PCR1 product. Then, the TSS PCR1 product is mixed with 1 μL Tn5-i5 primer (10 μM), 1 μL i7-anti-tag1 primer (10 μM), 15 μL KAPA HiFi

HotStart ReadyMix (2x), and Nuclease Free Water to reach a final volume of 30 μL. The reaction proceeds as follows: 98 ℃ for 3 min, 5 cycles of 98 ℃ for 20 s, 60 ℃ for 20 s, and 72 ℃ for 90 s, followed by 72 ℃ for 5 min. After purification using 1x AMPure XP beads, the resulting product is eluted with 10 μL Nuclease Free Water, yielding TSS PCR2 product. Next, the Nextera XT DNA Sample Preparation Kit (Illumina) is used for tagging. Specifically, the TSS PCR2 product is mixed with 1 μL of 10 μM Index 1 primer (N7), 1 μL of 10 μM Index 2 primer (N5), 15 μL KAPA HiFi HotStart ReadyMix (2x), and Nuclease Free Water to reach a final volume of 30 μL. The reaction proceeds as follows: 98 ℃ for 3 min, 4–10 cycles of 98 ℃ for 20 s, 55 ℃ for 20 s, and 72 ℃ for 90 s, followed by 72 ℃ for 5 min. After purification using 0.55x AMPure XP beads, the resulting product is eluted with 20 μL Nuclease Free Water, generating long fragment library. Furthermore, purification using 0.55x-0.9x AMPure XP beads is performed, and the product is eluted with 20 μL Nuclease Free Water, yielding short fragment library. The TES library construction method is similar to TSS, except that the anti-tag1 primer and i7-anti-tag1 primer in TSS are replaced with anti-TSO primer and i7-anti-TSO primer. Finally, the library is assessed using an Agilent Bioanalyzer 2100 or Qsep100™ automated nucleic acid and protein analysis system, and sequencing is performed on the Illumina NovaSeq 6000 platform using the PE150 model. For primer sequence information, please refer to the **Supplementary Table 1**.

Differentiation of human retinal organoids

In this study, we cultured human embryonic stem cells (hESCs, provided by Stem Cell Bank, Chinese Academy of Sciences) in Essential 8 (E8) medium on Vitronectin (VTN-N)-coated plates. To induce retinal differentiation, we dissociated hESC colonies using dispase and allowed them to form small cell clusters. Gradually, the medium was switched from E8 to neural induction medium (NIM) over a period of four days. The NIM contained DMEM/F12(1:1), N2 supplement (1%), MEM nonessential amino acids (1%), penicillin-streptomycin(1%), and heparin sulfate(2 mg/mL).To enhance the efficiency of retinal differentiation, we added recombinant human BMP4(50 ng/mL) starting from day 6. Every third day, we replaced half of the NIM volume with fresh NIM containing BMP4. On day 7, the cell aggregates were reseeded onto VTN-N-coated plates using NIM medium supplemented with 10% fetal bovine serum (FBS) and BMP4. On day 16, we manually dislodged the neural rosettes from the plates and maintained them in retinal differentiation medium (RDM) for the formation of retinal organoids. The RDM consisted of DMEM/F12 (3:1), B27 supplement (2%), MEM nonessential amino acids (2%), and penicillin-streptomycin (2%).Starting from day 30, we supplemented the RDM medium with 10% FBS, 100 μM taurine, 2 mM GlutaMAX, and 0.5 μM retinoic acid to support the long-term culture of retinal organoids[36,37].

scRCAT-seq2 library construction for D45 human retinal organoids

On day 45, we dissociated these organoids into single-cell suspensions by treating them with Accutase at 37°C for 30 minutes. The suspensions were then filtered through a 35-μm cell strainer, and the cells were resuspended in PBS containing 0.04% bovine serum albumin. Then, we used the Chromium Next GEM Single Cell Multiome ATAC + Gene Expression kit from 10x Genomics, following the manufacturer's

protocol to generate cDNA and scATAC libraries. 10 μL of cDNA is mixed with 1 μL of 10 μM read1 primer, 1 μL of 10 μM TSO-read1 primer, 15 μL of KAPA HiFi HotStart ReadyMix (2x), and the volume is supplemented with Nuclease Free Water to reach 30 μL. The reaction proceeds as follows: 98 ℃ for 3 min, 6–10 cycles of 98 ℃ for 20 s, 60 ℃ for 20 s, and 72 ℃ for 90 s, followed by 72 ℃ for 5 min. After purification using 1x AMPure XP beads, the resulting product is eluted with 10 μL Nuclease Free Water to obtain cDNA suitable for scRCAT-seq2. The TSS and TES library construction can be performed by replacing the corresponding primers in the 10x Genomics Chromium protocol.

Read alignments and gene expression estimation for ES cells

The original fastq files of ES cells undergo the following data preprocessing steps. Firstly, the UMI is identified based on the pattern "AACGCAGAGT + NNNNNNNNNNNN + AGTTAA" (oligo fragment + 12-base UMI + tag1 fragment). Then, for the TSS library, cDNA is identified using the pattern "CCCCAACCCT" (TSO fragment). For the TES library, the cDNA is trimmed to remove polyT tails (consecutive T segments with a base count > 10). As a result, the original paired-end reads are split into two single-end fastq files: one containing the UMI, and the other containing cDNA. Continuing with the analysis, zUMIs (version 2.9.4f) with STAR (version 2.7.9a) is used for sequence alignment and gene expression profiling. The reads are aligned to the human genome (hg38), and UMIs are merged using a Hamming distance of 1 to correct errors. The resulting bam files generated by zUMIs are further analyzed using deeptools (version 3.5.1) to calculate the coverage of reads on reference transcripts.

Read alignments and gene expression estimation for D45 human retinal organoids

The original fastq files undergo the following data preprocessing steps. Firstly, the UMI is identified based on the pattern "CTTCCGATCT + NNNNNNNNNNNNNNNN + NNNNNNNNNNNN + TTTTTT" (oligo fragment + 16-base barcode + 12-base UMI + polyT fragment). Then, for the TSS library, cDNA is identified using the pattern "CCCATGTACT" (reverse transcriptase + TSO fragment). For the TES library, the cDNA is trimmed to remove polyT tails (consecutive T segments with a base count > 10). As a result, the original paired-end reads are split into two single-end fastq files: one containing the barcode and UMI, and the other containing cDNA. Continuing with the analysis, zUMIs (version 2.9.4f) with STAR (version 2.7.9a) is used for sequence alignment and gene expression profiling. The reads are aligned to the human genome (hg38), then UMIs and barcodes are merged using a Hamming distance of 1 and a Barcode Binning of 2, respectively, to correct errors.

Reconstruction of RNA isoforms

The zUMIs-generated bam files were analyzed using the smart-seq3 workflow (https://github.com/sandberg-lab/Smart-seq3) to reconstruct RNA isoforms. The scRCAT-seq project (https://github.com/huyoujinlab/scRCAT-seq), employing random forest machine learning models, was utilized to predict false-positive TSS and TES events caused by factors such as premature termination

during reverse transcription, thereby enhancing the accuracy of reconstruction. Subsequently, TSS, TES, and intron endpoints of the reconstructed molecules were aligned to the positions of hg38 transcriptome annotation to assign them accordingly. A maximum deviation of 10 bases was allowed between the TSS, TES, and intron endpoints of the reconstructed molecules and the respective endpoints of the reference transcripts, considering them consistent with the reference. In evaluating the accuracy of reconstructed isoforms, those exhibiting complete agreement in TSS, TES, and all intron endpoints with a specific reference transcript were classified as full-length detected isoforms. Partial feature isoforms were defined as having some missing endpoints but matching other features to specific positions on a reference transcript, enabling their identification.

Data processing of ScISOr-seq data

The raw data obtained after SMRT sequencing was processed using the official SMRT software SMRT-Link and CCS for conversion and filtering to produced circular consensus reads (CCS data). Aligning the CCS data to the human genome (hg38) using minimap2 (version 2.17), the resulting alignments were further compared to hg38 transcriptome annotation using gffcompare (version 0.11.2) and collapse to remove redundancy.

Data analysis of scRICA-seq for the D45 human retinal organoids

The D45 human retinal organoids multimodal raw sequencing data was aligned to the human genome (hg38) using Cell Ranger (version 6.1.1), enabling analysis of gene expression and chromatin accessibility. Further analysis was conducted using the R packages Seurat (version 4.1.0) and Signac (version 1.6.0). Initially, a Seurat object was created based on the gene expression count matrix. Then, an ATAC-seq peak-count matrix was added as a Chromatin Assay to the Seurat object. Standardized methods were applied independently to preprocess and reduce the dimensionality of the two assays. For the Seurat assay, the data was normalized, and the "RunPCA" function was used for linear dimensionality reduction, selecting the top 50 principal components (1:50 dims) as parameters. Following that, the "RunUMAP" function was employed for nonlinear dimensionality reduction. Regarding the Chromatin assay, after normalizing the data, linear dimensionality reduction analysis using the "RunSVD" function was performed followed by nonlinear dimensionality reduction analysis using the "RunUMAP" function. The "RunUMAP" function was utilized with the parameters reduction = 'lsi' and dims = 2:50 to exclude the first dimension, which is typically correlated with sequencing depth. Afterwards, the "FindMultiModalNeighbors" function was employed to calculate the weighted nearest neighbor (WNN) graph, which represents the weighted combination of the RNA-seq and ATAC-seq modalities. This graph was subsequently used for UMAP visualization and clustering. The "FindAllMarkers" function was employed to identify marker genes for each cluster within the WNN object, with criteria of Log2FC > 0.25 and min.pct > 0.25. By comparing the identified markers with known early retinal development markers reported in the literature, cell type annotations were assigned to each cluster.

As the workflow described above, the SCRCAT2 zUMIs-generated gene expression matrix of D45 human retinal organoid was subjected to standard scRNA-seq downstream analysis using the R package Seurat.

Inference of pseudotime and trajectory

Monocle (version 2.27.0) was applied to unravel the lineage differentiation trajectories of early retinal cells. Firstly, a monocle object was created using the "as.CellDataSet" function. The "reduceDimension" function was applied to perform dimensionality reduction analysis using the DDRTree method, followed by pseudotime analysis using the "orderCells" function.

Identification of lineage-pioneering TFs

To identify key transcription factors involved in the early retina developmental trajectory, motif analysis was performed on the D45 human retinal organoids multimodal dataset to detect overrepresented motifs. Firstly, the "CreateMotifObject" function from the R package Signac was utilized to generate a motif object, which was then stored within the multimodal WNN object. Additionally, the "RegionStats" function was employed to calculate sequence characteristics of peaks, such as sequence length, GC content, and dinucleotide frequencies. The "FindMotifs" function from the R package chromVAR (version 1.16.0) was used to identify enriched transcription factor binding motifs in the dynamic promoter regions of peaks along the pseudotime trajectory. Finally, for visualization purposes, the predicted transcription factors were arranged in ascending order of p-values.

Data analysis of differential expression and differential accessibility

Differential expression and accessibility analysis between two cell types were performed using the "FindMarkers" function from the R package Seurat. The Wilcoxon rank-sum test was used to identify differentially expressed genes ($|\log_2(\text{fold change})| > 0.25$, adjusted p-value < 0.05), while a logistic regression framework was employed to determine differentially accessible peaks ($|\log_2(\text{fold change})| > 0.1$, p-value < 0.0005). Finally, a scatter plot will be generated using Pearson correlation to depict the correlation between the $\log_2$(fold change) values of expression and accessibility differences for genes that exhibit both significant differential expression and promoter region differential accessibility. A linear regression with a 95% confidence interval will also be added to the plot.

Peak annotation

We used the R package ChIPseeker[38] to map peaks to the nearest genes and gene regions. Promoter sites were defined as the TSS (Transcription Start Site) upstream 2000 bp and downstream 200 bp.

Data analysis of alternative TSS and TES

In order to identify alternative TSS and TES during differentiation from one cell type to another in early-stage retinal development, TSS and TES analysis were performed separately on the bam files generated by zUMIs from the D45 scRCAT-seq2 organoids data. For each gene that exists in both cell types

simultaneously, a 2x2 table was created by comparing the UMI counts of the major isoform and minor isoform in the two cell types. A Fisher's exact test was conducted on the table to identify genes with significant TSS/TES changes between the two cell types, using a threshold of p value < 0.05.

Data analysis of alternative splicing

The bam files generated by zUMIs from the 45-day scRCAT-seq2 organoid data were filtered based on barcodes to extract specific cell types. The extracted bam files of the selected cell types were then subjected to quantification of expression for alternative splicing events using rMATS (version 4.1.2). The Gencode gtf file (human hg38) was used for annotation purposes. The alternative splicing events were categorized into five types: Skipped exon, Alternative 5' splice site, Alternative 3' splice site, Retention Intron, and Mutually Exclusive Exons. The statistical model of rMATS employed a likelihood-ratio test to compute P-values, reflecting the differences in Inclusion Level between the two groups. The P-values were subsequently adjusted using the Benjamini-Hochberg algorithm to obtain False Discovery Rate (FDR) values.To visualize the results of the rMATS analysis, rmats2sashimiplot (version 2.0.4) was employed. Additionally, the R package bedtoolsR (version 2.30.0–2), which relies on bedtools (version 2.30.0), was used to identify overlapping regions between differential accessibility peaks and alternative splicing sites.

Declarations

Acknowledgement

This work was funded by the National Natural Science Foundation of China (32171445)；The Science and Technology Program of Guangzhou (202201020624)；"Precision Medicine and Stem Cells" Project of Key Field R&D Program of Guangdong province (2023B1111020006).

Contributions

Y.H., G.F. and S.Z. conceived and designed the study. S.Z., Y.X., Y.Q., Z.C., X.L., X.C., W.D. and J.C. performed experiments. Y.H., X.M., S.Z., Y.X., J.Z. and X.J. analyzed the data and performed statistical analyses. Y.H., S.Z., X.M. and Y.X. interpreted the data and wrote the manuscript in discussion with all authors.

Competing interests

The authors declare no competing interests.

References

1. Foster DS, Januszyk M, Delitto D et al (2022) Multiomic analysis reveals conservation of cancer-associated fibroblast phenotypes across species and tissue of origin. Cancer Cell 40(11):1392

2. Trevino AE, Müller F, Andersen J et al (2021) Chromatin and gene-regulatory dynamics of the developing human cerebral cortex at single-cell resolution. Cell 184(19):5053
3. Han M, Li F, Zhang Y et al (2022) FOXA2 drives lineage plasticity and KIT pathway activation in neuroendocrine prostate cancer. Cancer Cell 40(11):1306
4. Hu Y, Zhong J, Xiao Y et al (2020) Single-cell RNA cap and tail sequencing (scRCAT-seq) reveals subtype-specific isoforms differing in transcript demarcation, Nat Commun 11 (1)
5. Hu Y, Huang K, An Q et al (2016) Simultaneous profiling of transcriptome and DNA methylome from a single cell, Genome Biol 17 (1)
6. Fernandez-Suarez E, Gonzalez-Del PM, Garcia-Nunez A et al (2023) Expanding the phenotype of THRB: a range of macular dystrophies as the major clinical manifestations in patients with a dominant splicing variant. Front Cell Dev Biol 11:1197744
7. Wei M, Sun Y, Li S et al (2023) Single-cell profiling reveals Muller glia coordinate retinal intercellular communication during light/dark adaptation via thyroid hormone signaling. Protein Cell 14(8):603
8. Volkov LI, Kim-Han JS, Saunders LM et al (2020) Thyroid hormone receptors mediate two distinct mechanisms of long-wavelength vision, *Proc. Natl. Acad. Sci. U. S. A.* 117 (26), 15262
9. Assawachananont J, Kim SY, Kaya KD et al (2018) Cone-rod homeobox CRX controls presynaptic active zone formation in photoreceptors of mammalian retina. Hum Mol Genet 27(20):3555
10. Chau KY, Chen S, Zack DJ et al (2000) Functional domains of the cone-rod homeobox (CRX) transcription factor. J Biol Chem 275(47):37264
11. Kohl S, Coppieters F, Meire F et al (2012) A nonsense mutation in PDE6H causes autosomal-recessive incomplete achromatopsia. Am J Hum Genet 91(3):527
12. Piri N, Gao YQ, Danciger M et al (2005) A substitution of G to C in the cone cGMP-phosphodiesterase gamma subunit gene found in a distinctive form of cone dystrophy. Ophthalmology 112(1):159
13. Singh HP, Wang S, Stachelek K et al (2018) Developmental stage-specific proliferation and retinoblastoma genesis in RB-deficient human but not mouse cone precursors, *Proc. Natl. Acad. Sci. U. S. A.* 115 (40), E9391
14. Singh HP, Shayler D, Fernandez GE et al (2022) An immature, dedifferentiated, and lineage-deconstrained cone precursor origin of N-Myc-initiated retinoblastoma, *Proc. Natl. Acad. Sci. U. S. A.* 119 (28), e2094246177
15. Kurzawa-Akanbi M, Whitfield P, Burte F et al (2022) Retinal pigment epithelium extracellular vesicles are potent inducers of age-related macular degeneration disease phenotype in the outer retina. J Extracell Vesicles 11(12):e12295
16. Diacou R, Nandigrami P, Fiser A et al (2022) Cell fate decisions, transcription factors and signaling during early retinal development. Prog Retin Eye Res 91:101093
17. Martinez-Moreno CG, Epardo D, Balderas-Marquez JE et al (2019) Regenerative Effect of Growth Hormone (GH) in the Retina after Kainic Acid Excitotoxic Damage, Int J Mol Sci 20 (18)

18. Capone GT, Bendotti C, Oster-Granite ML et al (1991) Developmental expression of the gene encoding growth-associated protein 43 (Gap43) in the brains of normal and aneuploid mice. J Neurosci Res 29(4):449
19. Pan L, Deng M, Xie X et al (1981) ISL1 and BRN3B co-regulate the differentiation of murine retinal ganglion cells, *Development.* 135 (11), (2008)
20. Kobayashi T, Iwamoto Y, Takashima K et al (2015) Deubiquitinating enzymes regulate Hes1 stability and neuronal differentiation. Febs J 282(13):2411
21. Kautzman AG, Keeley PW, Nahmou MM et al (2018) Sox2 regulates astrocytic and vascular development in the retina. Glia 66(3):623
22. Liu Y, Hong W, Gong P et al (2023) Specific knockout of Sox2 in astrocytes reduces reactive astrocyte formation and promotes recovery after early postnatal traumatic brain injury in mouse cortex. Glia 71(3):602
23. Song WT, Zeng Q, Xia XB et al (2016) Atoh7 promotes retinal Muller cell differentiation into retinal ganglion cells. Cytotechnology 68(2):267
24. Miesfeld JB, Ghiasvand NM, Marsh-Armstrong B et al (2020) The Atoh7 remote enhancer provides transcriptional robustness during retinal ganglion cell development, *Proc. Natl. Acad. Sci. U. S. A.* 117 (35), 21690
25. Wu F, Bard JE, Kann J et al (2021) Single cell transcriptomics reveals lineage trajectory of retinal ganglion cells in wild-type and Atoh7-null retinas. Nat Commun 12(1):1465
26. Bai RY, Staedtke V, Lidov HG et al (2012) OTX2 represses myogenic and neuronal differentiation in medulloblastoma cells. Cancer Res 72(22):5988
27. Ibad RT, Quenech'Du N, Prochiantz A et al (2022) OTX2 stimulates adult retinal ganglion cell regeneration. Neural Regen Res 17(3):690
28. Kim HT, Kim SJ, Sohn YI et al (2015) Mitochondrial Protection by Exogenous Otx2 in Mouse Retinal Neurons. Cell Rep 13(5):990
29. Lewis SL, Khoo PL, Andrea DYR et al (2007) Genetic interaction of Gsc and Dkk1 in head morphogenesis of the mouse. Mech Dev 124(2):157
30. Saint-Jore B, Puech A, Heyer J et al (1998) Goosecoid-like (GSCL), a Candidate Gene for Velocardiofacial Syndrome, Is Not Essential for Normal Mouse Development. Hum Mol Genet 7(12):1841
31. Motahari Z, Moody SA, Maynard TM et al (2019) In the line-up: deleted genes associated with DiGeorge/22q11.2 deletion syndrome: are they all suspects? J Neurodev Disord 11(1):7
32. Anand D, Agrawal SA, Slavotinek A et al (2018) Mutation update of transcription factor genes FOXE3, HSF4, MAF, and PITX3 causing cataracts and other developmental ocular defects. Hum Mutat 39(4):471
33. Graw J (2017) From eyeless to neurological diseases. Exp Eye Res 156:5

34. Keren H, Lev-Maor G, Ast G (2010) Alternative splicing and evolution: diversification, exon definition and function. Nat Rev Genet 11(5):345
35. Blencowe BJ (2006) Alternative splicing: new insights from global analyses. Cell 126(1):37
36. Kuwahara A, Ozone C, Nakano T et al (2015) Generation of a ciliary margin-like stem cell niche from self-organizing human retinal tissue, Nat Commun 6 (1)
37. Mao X, An Q, Xi H et al (2019) Single-Cell RNA Sequencing of hESC-Derived 3D Retinal Organoids Reveals Novel Genes Regulating RPC Commitment in Early Human Retinogenesis. Stem Cell Rep 13(4):747
38. Yu G, Wang L, He Q (2015) ChIPseeker: an R/Bioconductor package for ChIP peak annotation, comparison and visualization. Bioinformatics 31(14):2382
39. Ramsköld D, Luo S, Wang Y et al (2012) Full-length mRNA-Seq from single-cell levels of RNA and individual circulating tumor cells. Nat Biotechnol 30(8):777
40. Picelli S, Faridani OR, Björklund ÅK et al (2014) Full-length RNA-seq from single cells using Smart-seq2. Nat Protoc 9(1):171
41. Hagemann-Jensen M, Ziegenhain C, Chen P et al (2020) Single-cell RNA counting at allele and isoform resolution using Smart-seq3. Nat Biotechnol 38(6):708
42. Gupta I, Collier PG, Haase B et al (2018) Single-cell isoform RNA sequencing characterizes isoforms in thousands of cerebellar cells. Nat Biotechnol 36(12):1197
43. Volden R, Palmer T, Byrne A et al (2018) Improving nanopore read accuracy with the R2C2 method enables the sequencing of highly multiplexed full-length single-cell cDNA, *Proceedings of the National Academy of Sciences* 115 (39), 9726
44. Philpott M, Watson J, Thakurta A et al (2021) Nanopore sequencing of single-cell transcriptomes with scCOLOR-seq. Nat Biotechnol 39(12):1517
45. Fan X, Tang D, Liao Y et al (2020) Single-cell RNA-seq analysis of mouse preimplantation embryos by third-generation sequencing, Plos Biol 18 (12), e3001017
46. Liao Y, Liu Z, Zhang Y et al (2023) High-throughput and high-sensitivity full-length single-cell RNA-seq analysis on third-generation sequencing platform, Cell Discov 9 (1)

Figures

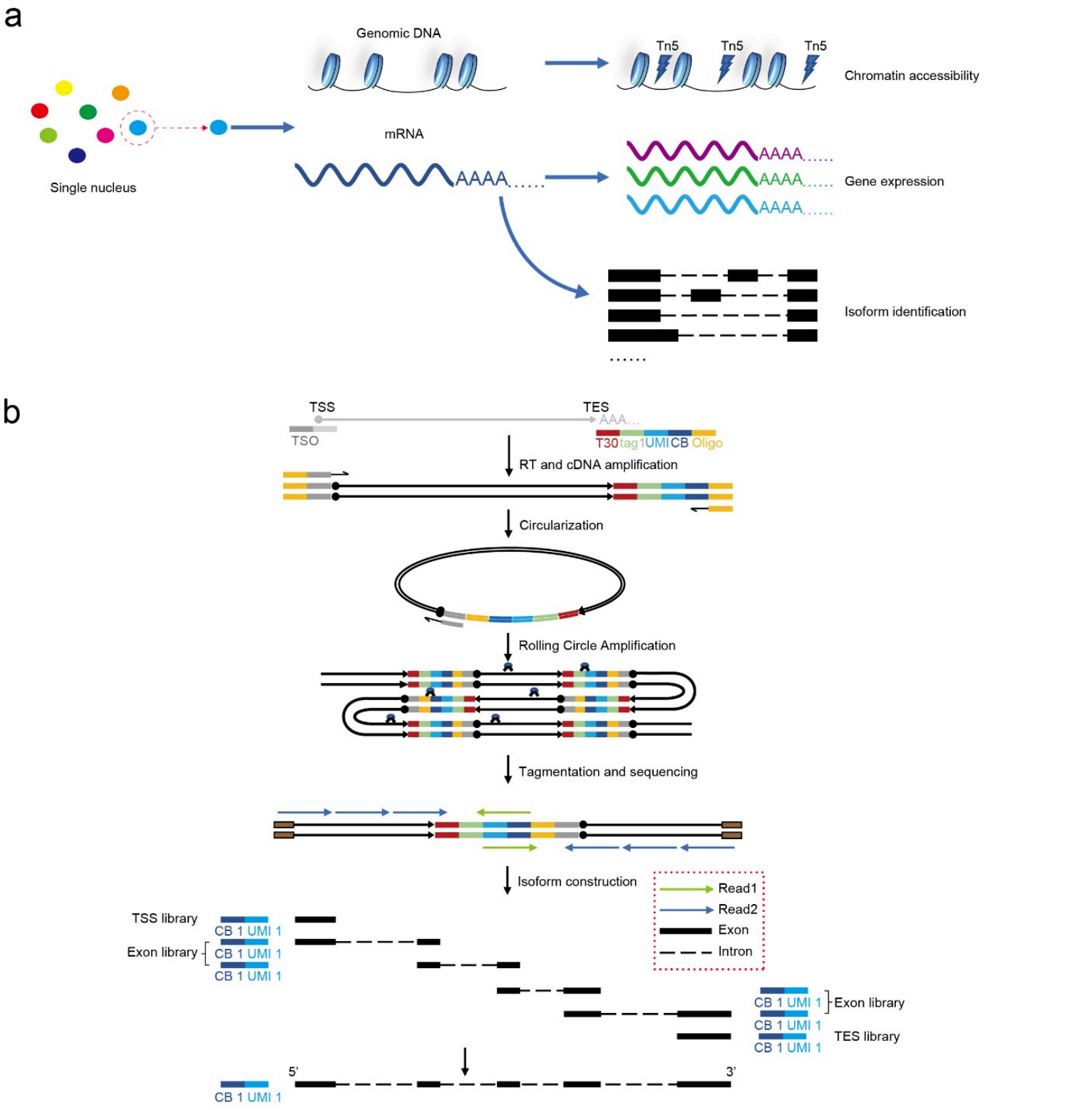

Figure 1

Overview of scRICA-seq. a, Schematic illustration of scRICA-seq to simultaneously profile the RNA isoforms and chromatin accessibility for the same single cell, by integrating the scRNA-seq, scATAC-seq, scRCAT-seq2. **b**, Schematic illustration of scRCAT-seq2 to depict the step-by-step procedure for generating the full-length cDNA library. CB: Cell barcode; TSO: Template-switching oligo; T30: 30 repeating T bases.

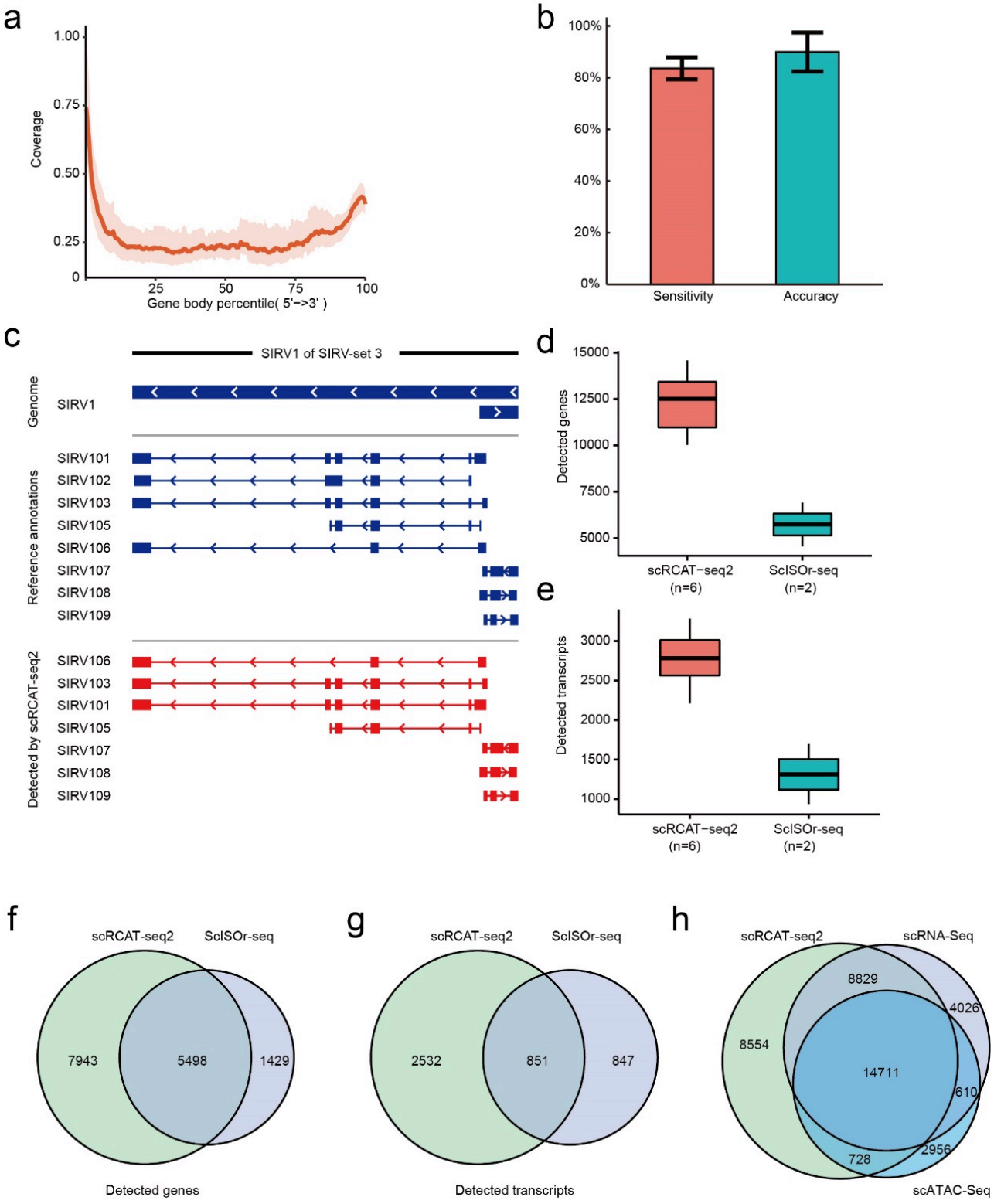

Figure 2

Performance of scRICA-seq. a, Coverage of scRICA-seq data on transcripts of single ES cells and SIRV-set 3 (n = 6). The displayed values represent averaged coverage of reads with shaded areas indicating standard deviations. **b**, Sensitivity and accuracy in identifying authentic reads aligning to the SIRV-set 3. Error bars represent standard deviation of the mean (n = 6). **c**, In SIRV-set 3, the gene SIRV1 is demonstrated as an example, where the full-length transcriptome was identified and constructed

through scRCAT-seq2. **d**,**e**, Comparison of the number of genes (**d**) and isoforms (**e**) detected by scRICA-seq and SMRT Sequencing in ES cells. **f**,**g**, Venn diagrams illustrating the overlap of genes (**f**) and isoforms (**g**) detected by scRCAT-seq2 and SMRT Sequencing. **h**, Venn diagram showing the overlaps between scRNA-seq, scATAC-seq and scRCAT-seq2 datasets.

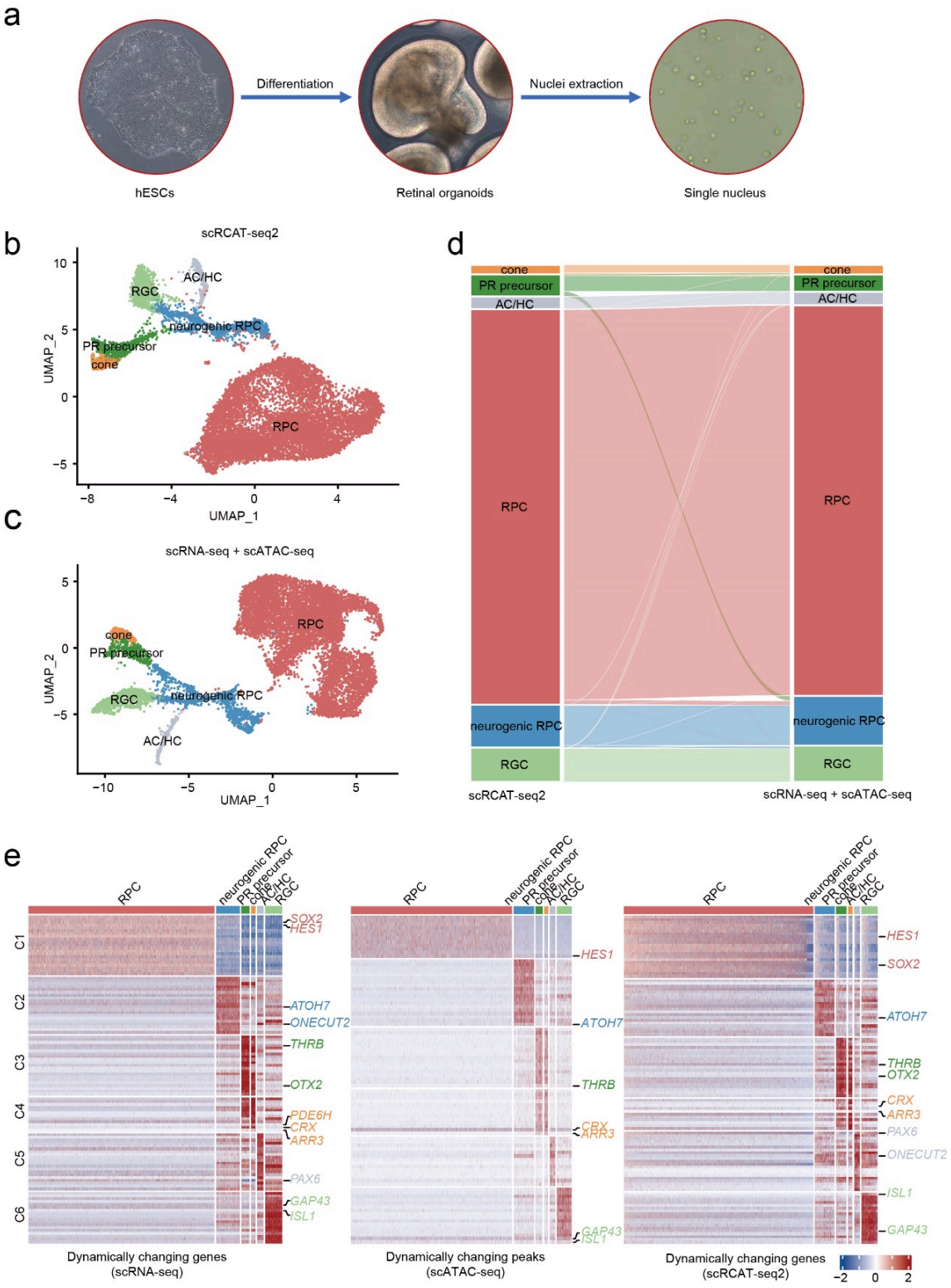

Figure 3

A multi-omics single-cell atlas of human retinal organoids based on scRICA-seq. a, Schematic illustration of organoid preparation and sample processing. Starting with culturing and differentiating hESCs into retinal organoids, followed by digestion to obtain single-cell suspensions, and the extraction of cell nuclei for library construction. **b**, Cell clustering of human retinal organoids with the scRICA-seq data. **c**, Cell clustering of human retinal organoid by using scATAC-seq and scRNA-seq. **d**, Matching the clusters identified by scRCAT-seq2 and scATAC-seq + scRNA-seq respectively. **e**, Heatmap displaying marker genes of each cluster detected by scRCAT-seq2, scATAC-seq and scRNA-seq respectively.

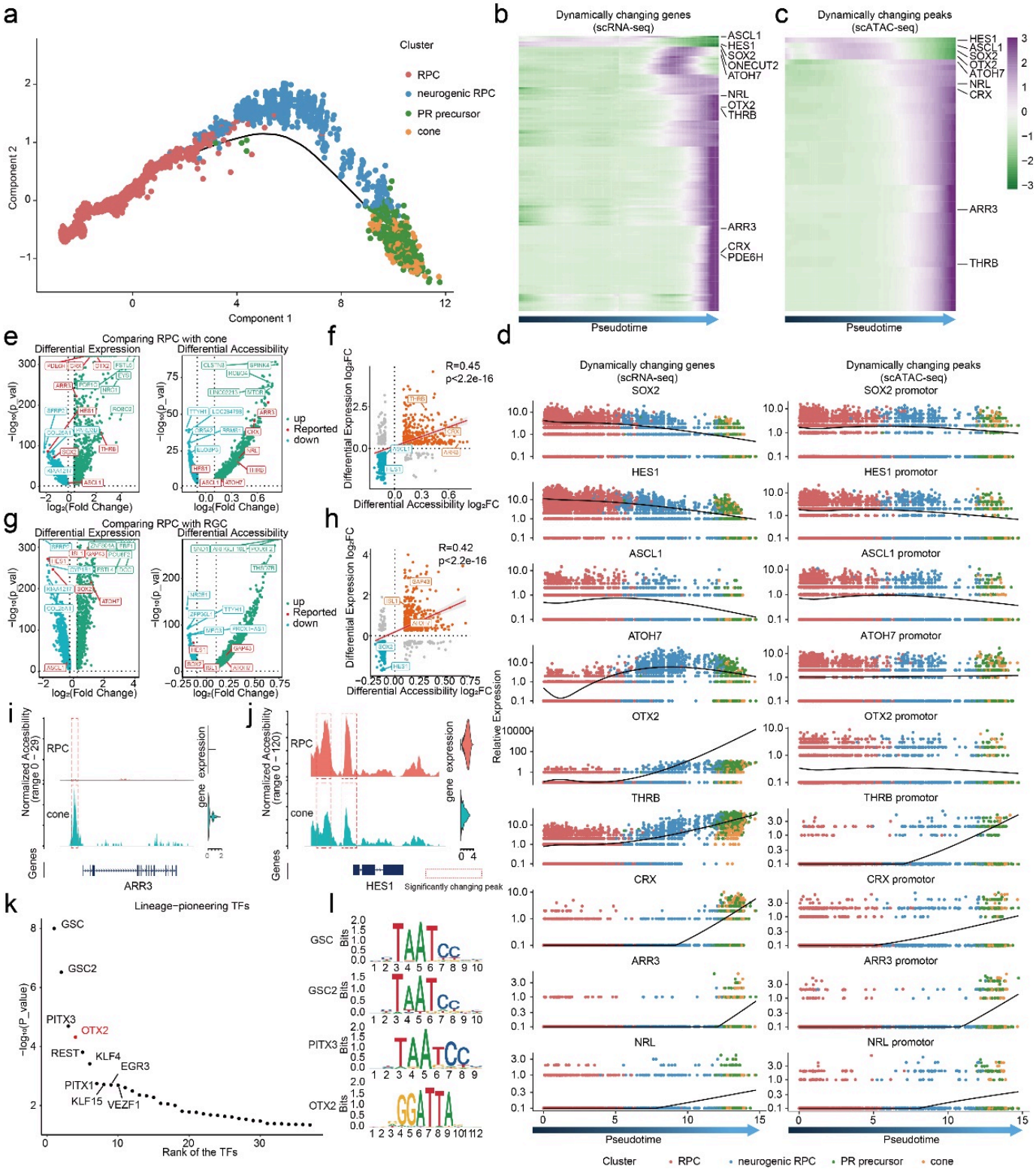

Figure 4

chromatin accessibility correlates with RNA transcription of fate determining factors of RPC. a, Trajectory map of RPC-cone development generated by pseudotime analysis of RPC, neurogenic RPC, PR precursor, and cone data. **b,**Heatmap of dynamic gene transcription during RPC-cone development. **c,**Heatmap of dynamic chromatin accessibility at gene promoters during RPC-cone development. **d,** Genes with concordant change in transcription level and chromatin accessibility during RPC-cone development. **e,** Volcano plot showing genes with changes in expression (left) and chromatin accessibility (right) between RPCs and cones. **f,** Correlation of gene expression with chromatin accessibility during RPC-Cone development. **g,** Volcano plot showing genes with concordant changes in expression (left) and chromatin accessibility (right) during RPC-RGC development. **h,** Correlation of gene expression with chromatin accessibility during RPC-RGC development. **i,j,**Schematic illustration of concordant gene expression and chromatin accessibility alterations in ARR3 (**i**) and HES1 (**j**) during RPC-cone development. **k,** Schematic representation of significantly changing transcription factors (TFs) during RPC-cone development. **l,**Examples of significantly changing transcription factors from (**k**).

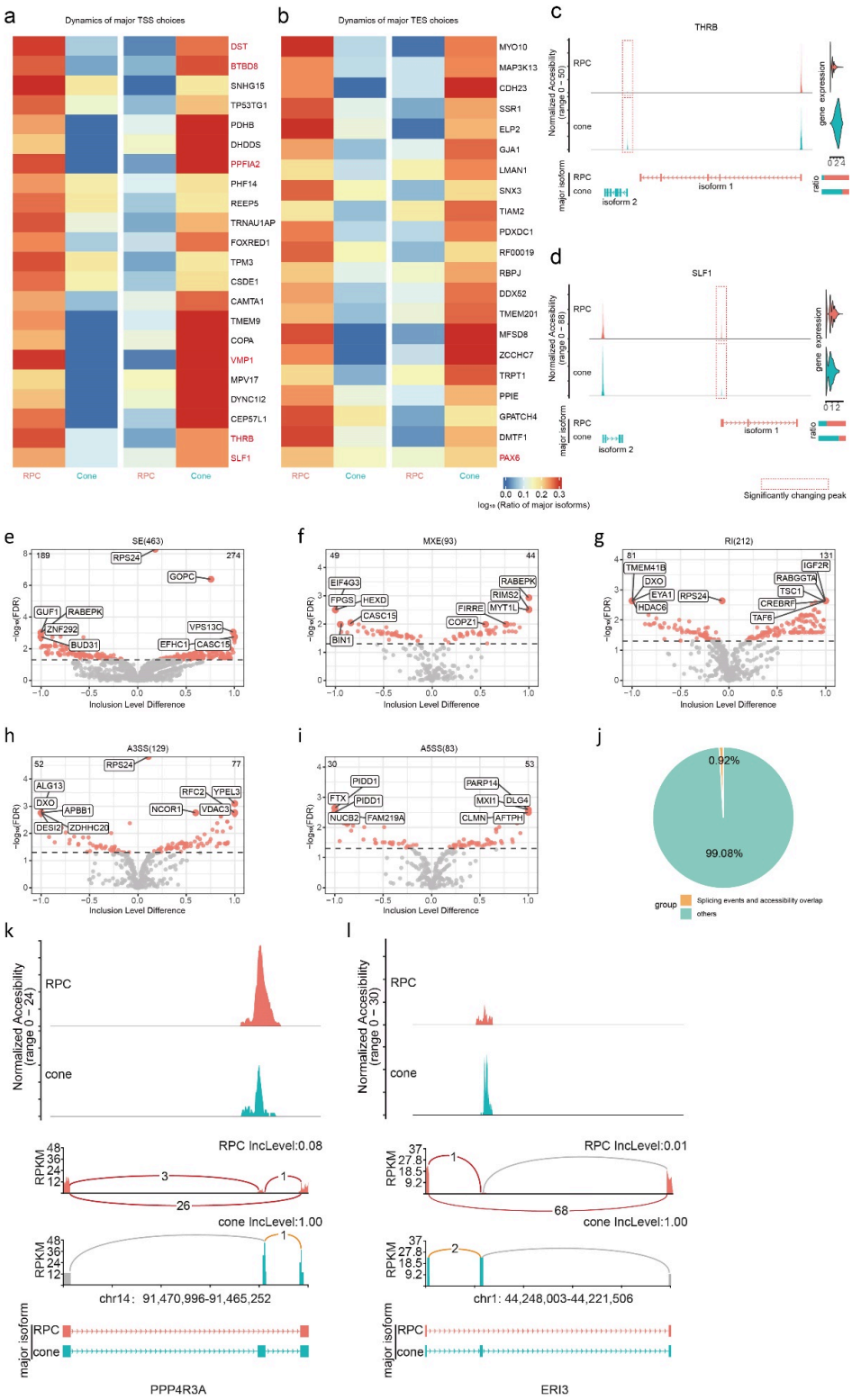

Figure 5

Correlation of RNA isoform choice with chromatin accessibility during RPC development. a,b, Heatmaps of the top 20 genes with differential TSS (**a**) or TES (**b**) choices in RPCs and cones, respectively. **c,d,** Schematic representation of the major isoform alteration in THRB and SLF1 differing in TSS during RPC-cone development. **e-i,**Volcano plots illustrating differential splicing events of SE (**e**), MXE (**f**), RI (**g**), A3SS (**h**), and A5SS (**i**) between RPCs and cones. **j,** Pie chart showing a small number of RNA alternative

splicing events associated with chromatin accessibility. **k,l,** Schematic representation of PPP4R3A (**k**) and ERI3 (**l**) locus undergoing SE with concurrent changes in chromatin accessibility. The gray peaks or lines in the schematic represent reads that were inferred based on the reference genome.

Supplementary Files

This is a list of supplementary files associated with this preprint. Click to download.

- SupplementaryTable1TableofscRICAseqprimers.xlsx
- SupplementaryTable2ComparisonofscRICAseqandothermethods.xlsx
- ExtendedDataFig.docx